Geophysical Research Letters

RESEARCH LETTER
10.1029/2019GL085208

Isopycnal Mixing Controls Deep Ocean Ventilation

C. S. Jones[1] and Ryan P. Abernathey[1]

[1]Lamont-Doherty Earth Observatory, Palisades, NY, USA

Abstract Climate models often parameterize isopycnal mixing by mesoscale eddies using a diffusion operator that acts in the isopycnal direction, multiplied by an isopycnal-mixing coefficient. The magnitude of this coefficient is uncertain, with observational estimates ranging from 10 to 10,000 m^2/s. In an idealized-geometry ocean model, the isopycnal-mixing coefficient is varied across a similar range without allowing the circulation to change: This leads to large changes in the ventilation of the deep ocean. Passive tracers are used to assess the impact of varying the isopycnal-mixing coefficient on water mass distributions. Increasing the isopycnal-mixing coefficient from 50 to 5,000 m^2/s leads to a 63% reduction in the amount of North Atlantic Deep Water and a doubling in the amount of Antarctic Bottom Water in the deep Pacific ocean. This change is associated with a 700-yr reduction in the ideal age of water in the deep Pacific ocean.

Plain Language Summary The ocean is full of eddies at the 100-km scale that stir tracers along surfaces of constant density. Climate models generally have coarse grids that are not able to resolve these ocean eddies. Instead, climate models represent this stirring using a diffusion operator along surfaces of constant density: This diffusion operator smooths out gradients in ocean tracers like temperature, salinity, oxygen, and nutrients. Based on currently available observations, it is unclear how large this diffusion operator should be in climate models. The results shown in this paper suggest that the amount of diffusion along surfaces of constant density influences the pathway along which water reaches the deep Pacific. Improving estimates of the size of this diffusion operator would probably increase the accuracy of climate models.

Key Points:
- Passive tracers are used to quantify the amount of deep water that originated in each region of the surface ocean
- Increasing the isopycnal-mixing coefficient reduces the fraction of NADW in the deep Pacific
- Increasing the isopycnal-mixing coefficient reduces the ideal age of water in the deep Pacific

Supporting Information:
- Supporting Information S1

Correspondence to:
C. S. Jones,
spencerj@ldeo.columbia.edu

Citation:
Jones, C. S., & Abernathey, R. P. (2019). Isopycnal mixing controls deep ocean ventilation. *Geophysical Research Letters*, *46*, 13,144–13,151. https://doi.org/10.1029/2019GL085208

Received 29 AUG 2019
Accepted 10 OCT 2019
Accepted article online 16 OCT 2019
Published online 16 NOV 2019

1. Introduction

Oceanic mesoscale eddies typically have spatial scales of less than 100 km. Because of their relatively small scales, these eddies are not resolved in coarse-resolution ocean and climate models. Instead, eddy transports are commonly parameterized using the Gent and McWilliams (1990) and Redi (1982) schemes. The Gent and McWilliams scheme parameterizes the advective transport of mesoscale eddies. In this parameterization, the strength of this advective transport is controlled by the slopes of local isopycnals and by the Gent-McWilliams coefficient. The Redi scheme parameterizes the diffusive effects of eddies using a diffusion operator that acts in the isopycnal direction, with the rate of diffusion set by an isopycnal-mixing coefficient, κ_{redi}.

It is numerically convenient to set the isopycnal-mixing coefficient to be equal to the Gent-McWilliams coefficient (Griffies, 1998): This choice was common in early studies that used these two parametrizations (e.g., Danabasoglu & Mc Williams, 1995; Dunne et al., 2012; Farneti et al., 2010). Recent work suggests that this simplification is unrealistic (Abernathey et al., 2013; Smith & Marshall, 2009; Vollmer & Eden, 2013) and that the isopycnal-mixing coefficient is generally larger than the Gent-McWilliams coefficient.

Observational estimates of the isopycnal-mixing coefficient vary widely. Groeskamp et al. (2017) derive a global value of around 12 m^2/s, whereas Lumpkin and Flament (2001) estimate the isopycnal-mixing coefficient to be in excess of 10,000 m^2/s near the surface of the North Pacific. Other observational studies find a variety of isopycnal-mixing coefficients between these two values (e.g., Armi & Stommel, 1983; Garabato et al., 2007; Ledwell et al., 1998; Roach et al., 2018; Tulloch et al., 2014). Spatial variations in isopycnal mixing may partially explain the wide range of these values: Values of the isopycnal-mixing coefficient are generally higher in the top 1,000 m than in the deep ocean (Cole et al., 2015). However, even globally averaged estimates of the isopycnal-mixing coefficient vary substantially.

Abernathey and Ferreira (2015) show that isopycnal mixing is a major factor in controlling the ventilation of the Southern Ocean. They find that stronger winds increase eddy kinetic energy, and larger eddy kinetic energy is associated with stronger isopycnal mixing. Here, we explore how changing the strength of isopycnal mixing affects the global distributions of deep water masses. Our results may have repercussions for interpreting paleo-oceanographic data in time periods with stronger winds, for example, during glacial periods in the Pleistocene (Stuut et al., 2002).

Uncertainty in the isopycnal-mixing coefficient is a possible source of error in predictions of heat and carbon uptake by global climate models. Gnanadesikan et al. (2015) found that increasing the Redi isopycnal-mixing coefficient from 400 to 2,400 m^2/s increases historical oceanic uptake of anthropogenic carbon by 15% in the GFDL ESM2Mc model. This increase in carbon uptake appears to be caused by a combination of factors, including reduced stratification in the North Pacific and changes to biological feedbacks, as well as an increase in along-isopycnal diffusion of carbon. In this paper, we isolate the direct effects of along-isopycnal diffusion on the tracer field by keeping the stratification and velocity fields constant and only modifying the isopycnal-mixing coefficient used to transport passive tracers.

Here, we examine how changing the isopycnal-mixing coefficient affects the composition and age of deep Pacific water. Observations suggest that the water in the deep Pacific is primarily composed of North Atlantic Deep Water (NADW) and Antarctic Bottom Water (AABW). Estimates of the fraction of NADW in the deep Pacific ocean vary, but Gebbie and Huybers (2010), Johnson (2008), and Broecker et al. (1998) all agree that this fraction is less than 50%. Observational estimates suggest that water takes about 1,300 yr to reach the deep North Pacific from the surface (Khatiwala et al., 2012).

Passive tracers are commonly used to characterize the age of water in ocean models (England, 1995; Holzer & Hall, 2000) but can also be used to characterize the fraction of water that was last ventilated in a chosen region of the surface (Haine & Hall, 2002; Primeau, 2005). Here, we use these tracers to characterize both the age of water in the deep ocean and the fraction of deep water that was last ventilated in a specific area of the surface ocean.

Our model uses 11 passive tracers, 10 of which represent water masses like NADW or AAIW and one of which represents the time since water was last in contact with the surface (ideal age). We change the Redi isopycnal-mixing coefficient for passive tracers only and examine the effects on the distributions of these tracers. The distribution of passive tracers for different Redi isopycnal-mixing coefficients and different vertical diffusivities is compared. Our results suggest that increasing the isopycnal-mixing coefficient reduces the fraction of NADW in the deep Pacific ocean and that tracer transport by isopycnal mixing is as important as tracer transport by vertical diffusivity for setting tracer concentrations in the deep ocean.

2. Methods

The Massachusetts Institute of Technology general circulation model (MITgcm; Marshall et al., 1997) is configured in an idealized-geometry two-basin ocean-only domain, similar to that used in Jones and Cessi (2016). This domain was chosen for its simplicity: The overturning and tracer concentrations in this domain are conveniently plotted in two panels (see below), enabling easy interpretation. In addition, this model's relatively inexpensive computational cost allowed us to use a large number of water-mass tracers.

The domain, which has 1° resolution, is a spherical sector spanning 70°S to 70°N in latitude and 210° in longitude. Two one-grid-point-wide continents run in the meridional direction, dividing the domain into a narrow basin, which represents the Atlantic, and a wide basin, which represents the Pacific. At the southern edge of the domain, the basins are joined by a reentrant channel that represents the Southern Ocean. The continent to the east of the Atlantic basin extends from 35°S to 70°N, while the continent to the west of the Atlantic basin extends from 52.5°S to 70°N. There is a ridge of height 1,333 m located directly south of the long continent, where a short wall that represents the Antarctic Peninsula extends from 70°S to 65°S.

The model is forced with zonally uniform wind stress, temperature relaxation, and freshwater flux, as shown in Figures 1a–1c, except in the cross-hatched region of Figure 1d. A uniform freshwater flux of -2×10^{-7} m/s is applied to the cross-hatched area, which represents a coastal polynya. (The inclusion of the polynya region is necessary to produce a lower-cell overturning of realistic strength.) The temperature used for surface temperature relaxation in this area is set to zero. The area integral of the freshwater flux over the domain is zero. As in Jones and Cessi (2016), the model uses a linear equation of state.

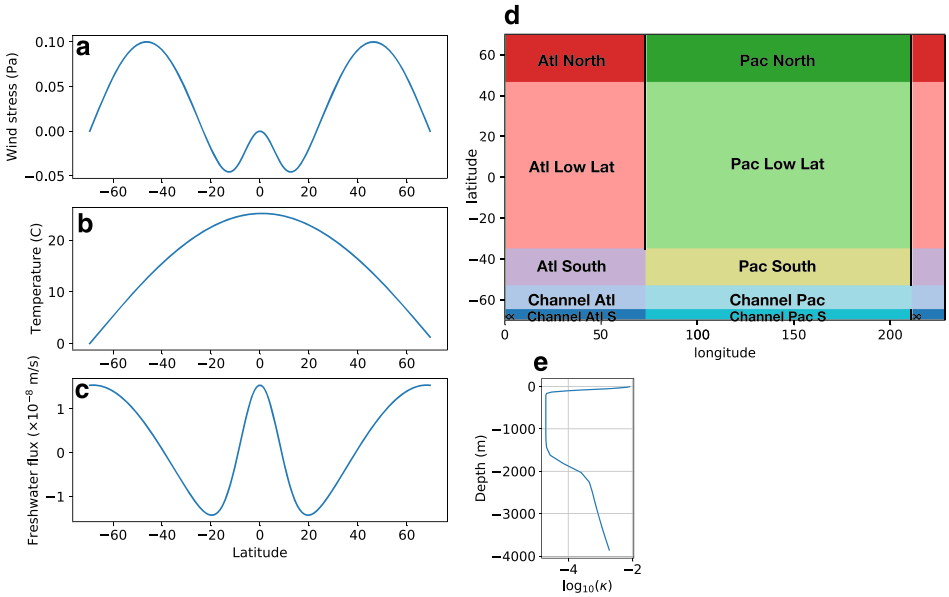

Figure 1. (a) Surface wind stress in pascals, (b) surface temperature relaxation profile in degrees Celsius, and (c) surface freshwater flux in $\times 10^{-8}$ m/s. (d) Surface regions associated with each of the passive tracers. The westernmost 20° of the domain is repeated on the right side of the domain. The concentration of each tracer is relaxed to one in its associated surface region and to zero at the surface outside this region. In the small cross-hatched region at 70°S and 0°E and repeated at 70°S and 210°E, the surface freshwater flux is set to -2×10^{-7} m/s, to simulate a polynya. (e) The original vertical diffusivity profile, used for temperature and salinity in all the experiments shown here.

In addition to temperature and salinity, the model has 10 water-mass tracers; each of these tracers is relaxed to one in a chosen region of the surface and to zero at the surface elsewhere. The surface regions associated with each of the passive tracers are shown in Figure 1d. Because the surface regions are nonoverlapping and together they cover the whole ocean surface, in equilibrium, the sum of all tracer concentrations is one at every point in the domain. At any given point, the concentration of each individual tracer is equal to the fraction of water that originated in the surface region that corresponds with that tracer. The tracer "Atl North" is associated with NADW, and the tracers "Channel Atl S" and "Channel Pac S" are associated with AABW. Besides the 10 water-mass tracers, we use an ideal age tracer, which is set to zero over the whole surface ocean and increases in concentration by one time unit per unit of time it spends away from the ocean surface.

Our experiments use the Prather (1986) second-order moments scheme and a vertical diffusivity profile of

$$\kappa = \kappa_v + \left[\kappa_{deep} + \kappa_{abyss}\left(10^{-(z+4{,}000)/2{,}000}\right)\right]\frac{\left[1-\tanh\left(\frac{z+2{,}000}{200}\right)\right]}{2} + 10^{-2}\frac{\left[1+\tanh\left(\frac{z+30}{30}\right)\right]}{2}. \quad (1)$$

This represents a high-diffusivity mixed layer above 30-m depth, below which the vertical diffusivity tapers to κ_v, increasing to $\kappa_{deep}+\kappa_v$ at 2,000 m, and $\kappa_{abyss}+\kappa_{deep}+\kappa_v$ near the bottom. For temperature and salinity, $\kappa_v = 2\times10^{-5}$ m^2/s, $\kappa_{deep} = 2\times10^{-4}$ m^2/s, and $\kappa_{abyss} = 2\times10^{-3}$ m^2/s. The vertical diffusivity profile for temperature and salinity is henceforth referred to as "the original vertical diffusivity profile"(see Figure 1e); it is similar to the vertical diffusivity profile used by Nadeau et al. (2019). This profile is very idealized but emulates an increase in vertical mixing below 2,000-m depth that is seen in observations (e.g., Nikurashin & Ferrari, 2013). Various different profiles of vertical diffusivity are used to transport passive tracers in our experiments.

The advective part of the tracer transport due to eddies is parameterized using the Gent and McWilliams (1990) scheme with a uniform Gent-McWilliams coefficient, $\kappa_{GM} = 500$ m^2/s. The diffusive part of the eddy transport is parameterized using Redi (1982). For temperature and salinity, the Redi isopycnal-mixing coefficient is $\kappa_{redi} = 500$ m^2/s. We vary the Redi coefficient used to transport passive tracers.

The values of κ^{tr}_{redi}, κ^{tr}_{v}, κ^{tr}_{deep}, and κ^{tr}_{abyss} are varied in six experiments, where the tr superscript indicates that these diffusivities are only applied to the water-mass and ideal age tracers. The first three experiments use

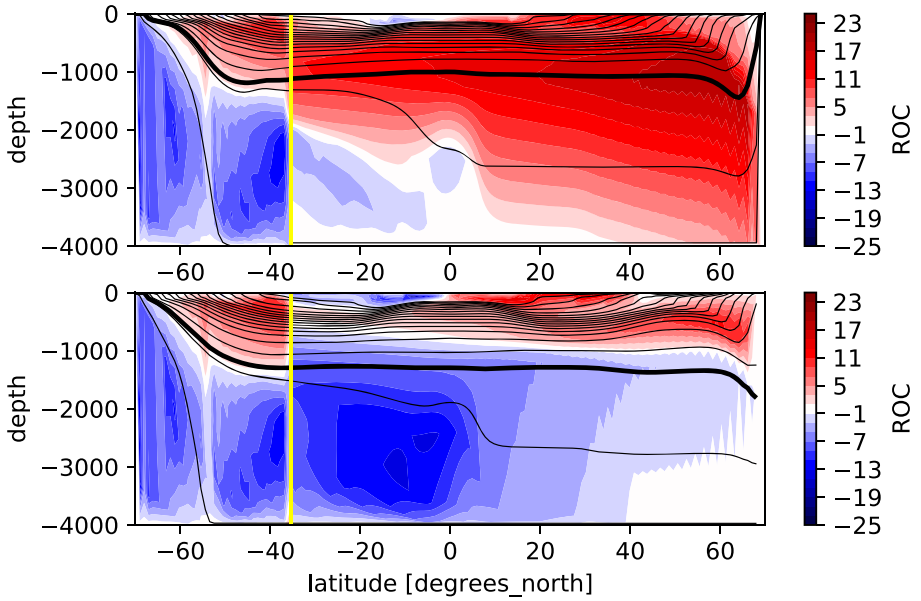

Figure 2. The residual overturning stream function (contour interval 2 Sv; color), calculated in density space and mapped back into depth space, as detailed in Jones and Cessi (2016), and the zonally averaged depth of buoyancy surfaces (contour interval 0.002 m^2/s; black) in the Atlantic basin (top) and the Pacific basin (bottom). South of the vertical yellow line that marks 35°S, the residual overturning stream function is zonally integrated over the whole domain. The thick black contour shows the isopycnal b_m, which approximately divides the northward flowing water in the upper Atlantic from the southward flowing water in the deep Atlantic. ROC = residual overturning circulation.

the original vertical diffusivity profile to transport these tracers, and κ^{tr}_{redi} is modified in each case: The first experiment has $\kappa^{tr}_{redi} = 50\ m^2/s$, the second has $\kappa^{tr}_{redi} = 500\ m^2/s$, and the third has $\kappa^{tr}_{redi} = 5,000\ m^2/s$. In the other three experiments, $\kappa^{tr}_{redi} = 500\ m^2/s$, but κ^{tr}_{v} is varied, and κ^{tr}_{deep} and κ^{tr}_{abyss} are set to zero (the vertical diffusivity of passive tracers is constant below the mixed layer). In the first of these experiments, $\kappa^{tr}_{v} = 2\times10^{-5}\ m^2/s$; in the second, $\kappa^{tr}_{v} = 2\times10^{-4} m^2/s$; and in the third, $\kappa^{tr}_{v} = 2\times10^{-3}\ m^2/s$. In each case, the model is run for at least 4,000 yr, until equilibrium is reached. The results shown below are averaged over the last 100 yr of the model run.

The velocities in all of these experiments are the same: The overturning is shown in Figure 2. Middepth isopycnals outcrop in the North Atlantic and in the Southern Ocean but not in the North Pacific. About 20 Sv of deep water is formed in the North Atlantic, consistent with estimates by Lumpkin and Speer (2007) and Talley (2013).

In our model, about 13 Sv of bottom water flows northward across 30°S. Because our idealized model only covers 210° in longitude, we do not expect it to form as much deep water as the real ocean. Most diffusive upwelling of deep water occurs between 30°S and 30°N: The area of our Pacific basin between these two latitudes is $9.7\times10^7\ km^2$, whereas the area of the real Pacific plus Indian Oceans in this latitude band is $1.5\times10^8\ km^2$. Our Atlantic is similar in size to the real Atlantic. About 10 Sv enters the Pacific basin at 30°S: If the basin were scaled up to the size of the real Pacific plus Indian Oceans, we would expect about 15 Sv to enter this basin, and a total of 18 Sv of bottom water would leave the Southern Ocean at 30°S. This is lower than the estimate of Lumpkin and Speer (2007), who find that 25.8 ± 6.5 Sv enters the ocean basins at 32°S. Sensitivity experiments (not shown) find that our conclusions are not affected by a 5-Sv reduction in the strength of Southern Ocean bottom water formation, implying that our results are robust even though our model produces too little bottom water.

Another interesting feature of the circulation in our model is that the abyssal cell is split in the Southern Ocean, with a minimum in the residual overturning circulation south of 55°S and another minimum north of this that extends into the basins (Figure 2). The presence of this split may indicate that a lot of NADW is entrained into the abyssal cell without reaching the surface, which is consistent with the distribution of NADW in Figure 3. Cessi (2019) shows that the abyssal cell in ECCOv4 is split, though to a lesser extent than

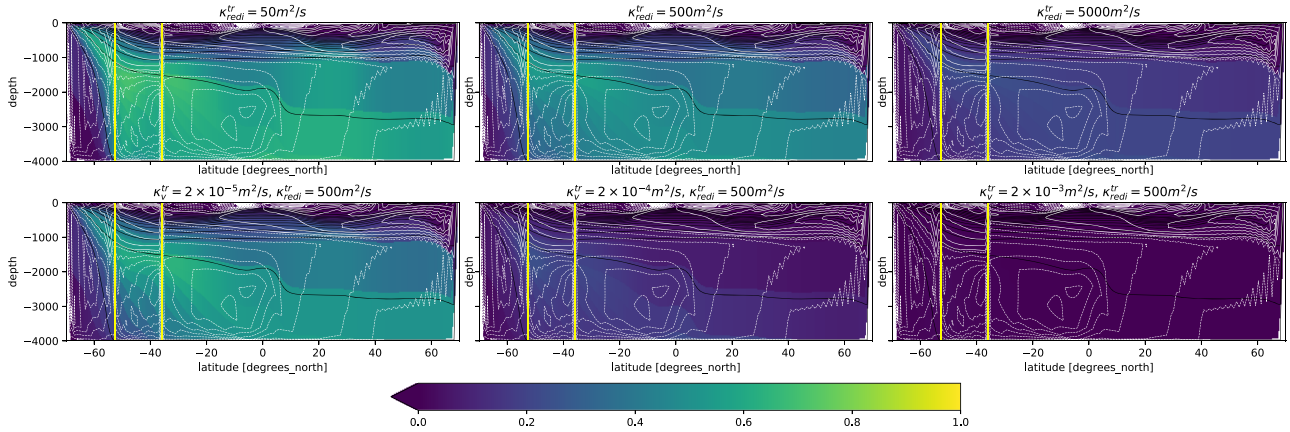

Figure 3. Concentration of the tracer that originates at the surface in the north of the Atlantic basin, averaged zonally over the Pacific basin (and over that sector of the reentrant channel) for $\kappa^{\mathrm{tr}}_{\mathrm{redi}} = 50\ \mathrm{m}^2/\mathrm{s}$ (top left), $\kappa^{\mathrm{tr}}_{\mathrm{redi}} = 500\ \mathrm{m}^2/\mathrm{s}$ (top middle), and $\kappa^{\mathrm{tr}}_{\mathrm{redi}} = 5{,}000\ \mathrm{m}^2/\mathrm{s}$ (top right), with the vertical diffusivity profile described above, and for $\kappa^{\mathrm{tr}}_{\mathrm{v}} = 2\times10^{-5}\ \mathrm{m}^2/\mathrm{s}$ (bottom left), $\kappa^{\mathrm{tr}}_{\mathrm{v}} = 2\times10^{-4}\ \mathrm{m}^2/\mathrm{s}$ (bottom middle), and $\kappa^{\mathrm{tr}}_{\mathrm{v}} = 2\times10^{-3}\ \mathrm{m}^2/\mathrm{s}$ (bottom right), with $\kappa^{\mathrm{tr}}_{\mathrm{redi}} = 500\ \mathrm{m}^2/\mathrm{s}$. The zonal average is performed in buoyancy coordinates, and the result transformed back into depth coordinates. The white contours show the residual overturning circulation, zonally integrated over the Pacific basin north of 35°S, and zonally integrated across the whole domain south of 35°S, with contours every 2 Sv. The black contours show the depth of buoyancy surfaces, zonally averaged across the Pacific basin or that sector of the channel with contour interval $0.002\ \mathrm{m}^2/\mathrm{s}$. The vertical yellow lines show the locations of the end of the short continent, at 35°S, and the end of the long continent, at 52.5°S.

ours, and Lumpkin and Speer (2007) show a similar split cell in their observational estimate of the residual overturning circulation.

3. Results

Figure 3 shows the concentration of tracer "Atl North," which represents NADW, in the wide basin. The distributions of NADW for $\kappa^{\mathrm{tr}}_{\mathrm{redi}} = 50\ \mathrm{m}^2/\mathrm{s}$ and $\kappa^{\mathrm{tr}}_{\mathrm{redi}} = 500\ \mathrm{m}^2/\mathrm{s}$ are similar: In these simulations NADW makes up about 50–60% of the water in the deep Pacific. AABW makes up 20–35% of this water, as discussed later. Modern observations show that deep Pacific waters are composed primarily of NADW and AABW, but the relative proportions of these water masses are much debated (Broecker et al., 1998; Gebbie & Huybers, 2010; Johnson, 2008). Increasing $\kappa^{\mathrm{tr}}_{\mathrm{redi}}$ to $5{,}000\ \mathrm{m}^2/\mathrm{s}$ reduces the concentration of NADW in the Pacific ocean. With this value of $\kappa^{\mathrm{tr}}_{\mathrm{redi}}$, NADW is mixed upward and southward along isopycnals more efficiently, toward the surface of the Southern Ocean, which is a sink of NADW.

The bottom panel of Figure 4 shows the concentration of each tracer below 2,000 m and north of the equator in the Pacific basin. For all of the experiments that use the original vertical diffusivity profile, about 15% of the water in the chosen region of the deep Pacific was last ventilated in the north of the Pacific basin, regardless of the value of the isopycnal-mixing coefficient (the forest green portion of the left three bars in the bottom panel of Figure 4). When $\kappa^{\mathrm{tr}}_{\mathrm{redi}} = 50\ \mathrm{m}^2/\mathrm{s}$, 60% of water in the chosen region originates in the North Atlantic, and 20% originates in the Southern Ocean. When $\kappa^{\mathrm{tr}}_{\mathrm{redi}} = 500\ \mathrm{m}^2/\mathrm{s}$, 49% of water in the chosen region originates in the North Atlantic, and 33% originates in the Southern Ocean. Increasing $\kappa^{\mathrm{tr}}_{\mathrm{redi}}$ from 500 to $5{,}000\ \mathrm{m}^2/\mathrm{s}$ leads to a much smaller fraction of NADW (22%) and a much larger fraction of AABW (62%).

Increasing $\kappa^{\mathrm{tr}}_{\mathrm{redi}}$ is associated with a reduction in the ideal age of water in the deep Pacific, as shown in the top panel of Figure 4. With the original vertical diffusivity profile, the ideal age of water in the Pacific north of the equator and below 2,000 m is 1,600 yr for $\kappa^{\mathrm{tr}}_{\mathrm{redi}} = 50\ \mathrm{m}^2/\mathrm{s}$, 1,400 yr for $\kappa^{\mathrm{tr}}_{\mathrm{redi}} = 500\ \mathrm{m}^2/\mathrm{s}$, and 700 yr for $\kappa^{\mathrm{tr}}_{\mathrm{redi}} = 5{,}000\ \mathrm{m}^2/\mathrm{s}$. It appears that larger $\kappa^{\mathrm{tr}}_{\mathrm{redi}}$ is associated with stronger mixing of AABW along isopycnals into the deep Pacific: AABW reaches the deep Pacific more quickly, reducing the ideal age there.

The Peclet number on isopycnals is approximately $\kappa^{\mathrm{tr}}_{\mathrm{redi}}/UL$, where U is the characteristic velocity and L is the characteristic length scale of the flow. The Peclet number is often used to quantify the relative importance of advective and diffusive transports. The average velocity in the southward flowing lower limb of the upper cell in the Atlantic is about 0.001 m/s, so taking a length scale of 4,000 km (about the width of the channel), the Peclet number is approximately 0.0125 for $\kappa^{\mathrm{tr}}_{\mathrm{redi}} = 50\ \mathrm{m}^2/\mathrm{s}$, 0.125 for $\kappa^{\mathrm{tr}}_{\mathrm{redi}} = 500\ \mathrm{m}^2/\mathrm{s}$, and 1.25 for $\kappa^{\mathrm{tr}}_{\mathrm{redi}} = 5{,}000\ \mathrm{m}^2/\mathrm{s}$. In other words, compared to the advective transport, the diffusive transport of water-mass tracers along isopycnals is small when $\kappa^{\mathrm{tr}}_{\mathrm{redi}} = 50\ \mathrm{m}^2/\mathrm{s}$ and $\kappa^{\mathrm{tr}}_{\mathrm{redi}} = 500\ \mathrm{m}^2/\mathrm{s}$, but the diffusive transport

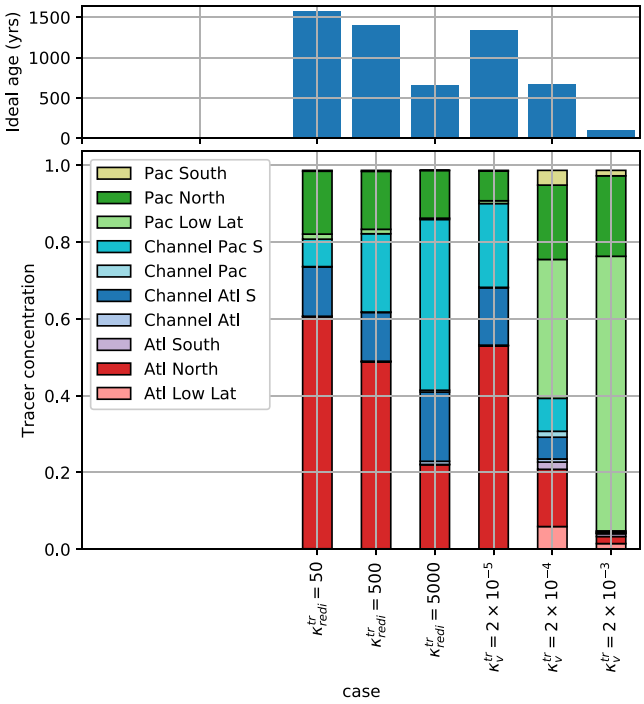

Figure 4. Ideal age in years (top) and average tracer concentration (bottom) in the Pacific basin north of the equator and below 2,000-m depth. Figure 1 shows the regions associated with each water-mass tracer. The left three bars represent experiments that use $\kappa^{tr}_{v} = 2 \times 10^{-5}$ m^2/s, $\kappa^{tr}_{deep} = 2 \times 10^{-4}$ m^2/s, and $\kappa^{tr}_{abyss} = 2 \times 10^{-3}$ m^2/s. The right three bars represent experiments that use $\kappa^{tr}_{deep} = 0$ m^2/s, $\kappa^{tr}_{abyss} = 0$ m^2/s, and $\kappa^{tr}_{redi} = 500$ m^2/s.

becomes significant when $\kappa^{tr}_{redi} = 5,000$ m^2/s, apparently leading to a large change in the fraction of NADW in the deep Pacific ocean.

The concentration of NADW in the deep Pacific also declines when κ^{tr}_{v} is increased from 2×10^{-5} to 2×10^{-4} m^2/s (cf. the bottom left and bottom middle panels of Figure 3). Increasing κ^{tr}_{v} from 2×10^{-5} to 2×10^{-4} m^2/s creates similar changes in the NADW fraction in the deep Pacific to increasing κ^{tr}_{redi} from 500 to 5,000 m^2/s. This suggests that when comparing the direct effect of each diffusion coefficient on tracer transport, the isopycnal-mixing coefficient is as important as the vertical diffusivity for regulating global tracer distributions.

When the vertical diffusivity is increased from $\kappa^{tr}_{v} = 2 \times 10^{-5}$ to 2×10^{-4} m^2/s, NADW concentration is preferentially reduced at shallower depths (cf. bottom left and bottom middle panels of Figure 3). In the experiments with higher vertical diffusivities, "Pac Low Lat" and "Pac North" tracers are mixed directly downward from the surface, occupying a large fraction of the deep Pacific ocean (green colors in Figure 4), and displacing NADW at shallower depths. Increasing κ^{tr}_{v} to 2×10^{-3} m^2/s completely removes NADW from the Pacific basin (bottom right panel of Figure 3). This NADW is replaced by water that is transported directly downward from the surface by the high vertical diffusivity.

The ideal age in the deep Pacific is 100 yr for $\kappa^{tr}_{v} = 2 \times 10^{-3}$ m^2/s, 700 yr for $\kappa^{tr}_{v} = 2 \times 10^{-4}$ m^2/s, and 1,300 yr for $\kappa^{tr}_{v} = 2 \times 10^{-5}$ m^2/s. A high vertical diffusivity enables very fast mixing of water downward from the surface and reduces the ideal age of water at depth.

4. Summary and Discussion

In our idealized model, increasing the isopycnal-mixing coefficient from $\kappa^{tr}_{redi} = 500$ to $\kappa^{tr}_{redi} = 5,000$ m^2/s reduces the concentration of NADW in the deep Pacific ocean by 55% and reduces the ideal age in the deep Pacific by 600 yr. Until recently, the isopycnal-mixing coefficient was neglected in discussions of the accuracy of global climate models, but our results indicate that the tracer transport by the isopycnal-mixing coefficient is as important as the tracer transport by the vertical diffusivity for setting the distribution of water masses in the deep ocean.

The magnitude of κ_{redi} is not well constrained by observations: All the values of κ^{tr}_{redi} used in our experiments are within the observational range. The different water mass distributions found in this paper suggest that uncertainty in the magnitude of κ_{redi} may be associated with disagreement in climate model predictions of carbon and heat storage in the deep ocean. Further work is needed to assess how spatial variability in κ_{redi} affects global tracer transport.

It may be possible to use an inverse model to estimate the value of κ_{redi} based on observations of various ocean tracers. Forget et al. (2015) estimate κ_{redi} for temperature and salinity by assimilating temperature, salinity, and velocity observations in the ECCOv4 model, although there is still high uncertainty in the deep ocean due to limited observations. Our results suggest that the same process could be performed with other tracers like PO_4^*, oxygen, and radiocarbon.

Our results may also have implications for interpreting paleo-oceanographic data. During glacial periods in the Pleistocene, the influence of NADW in the deep Atlantic was reduced. This is often attributed to a reduction in Lower NADW production (e.g., Oppo et al., 1995). However, there is also evidence that winds over the Atlantic were stronger during glacial periods in the Pleistocene (Stuut et al., 2002). Stronger winds are generally associated with higher eddy kinetic energy and a larger isopycnal-mixing coefficient (Meredith et al., 2012). A possible alternative explanation for the diminished influence of NADW in the deep Atlantic during these glacial periods is that elevated isopycnal mixing caused by stronger winds may have brought Southern Ocean waters further northward, reducing the concentration of NADW in the deep Atlantic.

Acknowledgments
C. S. J. is funded by the Lamont Postdoctoral Fellowship. R. P. A. acknowledges support from NSF Award OCE 1553593. The authors would like to thank Malte Jansen, David Munday, and one anonymous reviewer for comments that helped us to improve the paper. Code is available online (https://github.com/cspencerjones/tracers_two_basin/), with data (https://doi.org/10.6084/m9.figshare.7952465.v2). Xarray (Hoyer & Hamman, 2017) and other software tools supported by the Pangeo Project (NSF Award OCE 1740648) were used to perform data analysis and visualization.

References

Abernathey, R., & Ferreira, D. (2015). Southern Ocean isopycnal mixing and ventilation changes driven by winds. *Geophysical Research Letters*, *42*, 10–357. https://doi.org/10.1002/2015GL066238

Abernathey, R., Ferreira, D., & Klocker, A. (2013). Diagnostics of isopycnal mixing in a circumpolar channel. *Ocean Modelling*, *72*, 1–16. https://doi.org/10.1016/j.ocemod.2013.07.004

Armi, L., & Stommel, H. (1983). Four views of a portion of the North Atlantic subtropical gyre. *Journal of Physical Oceanography*, *13*(5), 828–857. https://doi.org/10.1175/1520-0485(1983)013<0828:FVOAPO>2.0.CO;2

Broecker, W., Peacock, S., Walker, S., Weiss, R., Fahrbach, E., Schröder, M., et al. (1998). How much deep water is formed in the Southern Ocean? *Journal of Geophysical Research*, *103*(C8), 15,833–15,843. https://doi.org/10.1029/98JC00248

Cessi, P. (2019). The global overturning circulation. *Annual review of marine science*, *11*, 249–270.

Cole, S. T., Wortham, C., Kunze, E., & Owens, W. B. (2015). Eddy stirring and horizontal diffusivity from Argo float observations: Geographic and depth variability. *Geophysical Research Letters*, *42*, 3989–3997. https://doi.org/10.1002/2015GL063827

Danabasoglu, G., & Mc Williams, J. C. (1995). Sensitivity of the global ocean circulation to parameterizations of mesoscale tracer transports. *Journal of Climate*, *8*(12), 2967–2987. https://doi.org/10.1175/1520-0442(1995)008<2967:SOTGOC>2.0.CO;2

Dunne, J. P., John, J. G., Adcroft, A. J., Griffies, S. M., Hallberg, R. W., Shevliakova, E., et al. (2012). GFDLs ESM2 global coupled climate–carbon earth system models. Part I: Physical formulation and baseline simulation characteristics. *Journal of Climate*, *25*(19), 6646–6665. https://doi.org/10.1175/JCLI-D-11-00560.1

England, M. H. (1995). The age of water and ventilation timescales in a global ocean model. *Journal of Physical Oceanography*, *25*(11), 2756–2777. https://doi.org/10.1175/1520-0485(1995)025h2756:TAOWAVi2.0.CO;2

Farneti, R., Delworth, T. L., Rosati, A. J., Griffies, S. M., & Zeng, F. (2010). The role of mesoscale eddies in the rectification of the Southern Ocean response to climate change. *Journal of Physical Oceanography*, *40*(7), 1539–1557. https://doi.org/10.1175/2010JPO4353.1

Forget, G., Ferreira, D., & Liang, X. (2015). On the observability of turbulent transport rates by Argo: Supporting evidence from an inversion experiment. *Ocean Science*, *11*(5), 839–853. https://doi.org/10.5194/os-11-839-2015

Garabato, A. C. N., Stevens, D. P., Watson, A. J., & Roether, W. (2007). Short-circuiting of the overturning circulation in the Antarctic Circumpolar Current. *Nature*, *447*(7141), 194. https://doi.org/10.1038/nature05832

Gebbie, G., & Huybers, P. (2010). Total matrix intercomparison: A method for determining the geometry of water-mass pathways. *Journal of Physical Oceanography*, *40*(8), 1710–1728. https://doi.org/10.1175/2010JPO4272.1

Gent, P. R., & McWilliams, J. C. (1990). Isopycnal mixing in ocean circulation models. *Journal of Physical Oceanography*, *20*(1), 150–155. https://doi.org/10.1175/1520-0485(1990)020h0150:IMIOCMi2.0.CO;2

Gnanadesikan, A., Pradal, M.-A., & Abernathey, R. (2015). Isopycnal mixing by mesoscale eddies significantly impacts oceanic anthropogenic carbon uptake. *Geophysical Research Letters*, *42*, 4249–4255. https://doi.org/10.1002/2015GL064100

Griffies, S. M. (1998). The Gent–McWilliams skew flux. *Journal of Physical Oceanography*, *28*(5), 831–841. https://doi.org/10.1175/1520-0485(1998)028h0831:TGMSFi2.0.CO;2

Groeskamp, S., Sloyan, B. M., Zika, J. D., & McDougall, T. J. (2017). Mixing inferred from an ocean climatology and surface fluxes. *Journal of Physical Oceanography*, *47*(3), 667–687. https://doi.org/10.1175/JPO-D-16-0125.1

Haine, T. W., & Hall, T. M. (2002). A generalized transport theory: Water-mass composition and age. *Journal of Physical Oceanography*, *32*(6), 1932–1946. https://doi.org/10.1175/1520-0485(2002)032h1932:AGTTWMi2.0.CO;2

Holzer, M., & Hall, T. M. (2000). Transit-time and tracer-age distributions in geophysical flows. *Journal of the Atmospheric Sciences*, *57*(21), 3539–3558. https://doi.org/10.1175/1520-0469(2000)057h3539:TTATADi2.0.CO;2

Hoyer, S., & Hamman, J. J. (2017). xarray: N-D labeled arrays and datasets in Python. *Journal of Open Research Software*, *5*, 10. https://doi.org/10.5334/jors.148

Johnson, G. C. (2008). Quantifying Antarctic Bottom Water and North Atlantic Deep Water volumes. *Journal of Geophysical Research*, *113*, C05027. https://doi.org/10.1029/2007JC004477

Jones, C. S., & Cessi, P. (2016). Interbasin transport of the meridional overturning circulation. *Journal of Physical Oceanography*, *46*(4), 1157–1169. https://doi.org/10.1175/JPO-D-15-0197.1

Khatiwala, S., Primeau, F., & Holzer, M. (2012). Ventilation of the deep ocean constrained with tracer observations and implications for radiocarbon estimates of ideal mean age. *Earth and Planetary Science Letters*, *325*, 116–125. https://doi.org/10.1016/j.epsl.2012.01.038

Ledwell, J. R., Watson, A. J., & Law, C. S. (1998). Mixing of a tracer in the pycnocline. *Journal of Geophysical Research*, *103*(C10), 21,499–21,529. https://doi.org/10.1029/98JC01738

Lumpkin, R., & Flament, P. (2001). Lagrangian statistics in the central North Pacific. *Journal of Marine Systems*, *29*(1-4), 141–155. https://doi.org/10.1016/S0924-7963(01)00014-8

Lumpkin, R., & Speer, K. (2007). Global ocean meridional overturning. *Journal of Physical Oceanography*, *37*(10), 2550–2562. https://doi.org/10.1175/JPO3130.1

Marshall, J., Adcroft, A., Hill, C., Perelman, L., & Heisey, C. (1997). A finite-volume, incompressible Navier Stokes model for studies of the ocean on parallel computers. *Journal of Geophysical Research*, *102*, 5753–5766. https://doi.org/10.1029/96JC02775

Meredith, M. P., Naveira Garabato, A. C., Hogg, A. M., & Farneti, R. (2012). Sensitivity of the overturning circulation in the southern ocean to decadal changes in wind forcing. *Journal of Climate*, *25*(1), 99–110. https://doi.org/10.1175/2011JCLI4204.1

Nadeau, L.-P., Ferrari, R., & Jansen, M. F. (2019). Antarctic sea ice control on the depth of North Atlantic Deep Water. *Journal of Climate*, *32*(9), 2537–2551.

Nikurashin, M., & Ferrari, R. (2013). Overturning circulation driven by breaking internal waves in the deep ocean. *Geophysical Research Letters*, *40*, 3133–3137. https://doi.org/10.1002/grl.50542

Oppo, D. W., Raymo, M. E., Lohmann, G. P., Mix, A. C., Wright, J. D., & Prell, W. L. (1995). A δ^{13}C record of Upper North Atlantic Deep Water during the past 2.6 million years. *Paleoceanography and Paleoclimatology*, *10*(3), 373–394. https://doi.org/10.1029/95PA00332

Prather, M. J. (1986). Numerical advection by conservation of second-order moments. *Journal of Geophysical Research*, *91*(D6), 6671–6681. https://doi.org/10.1029/JD091iD06p06671

Primeau, F. (2005). Characterizing transport between the surface mixed layer and the ocean interior with a forward and adjoint global ocean transport model. *Journal of Physical Oceanography*, *35*(4), 545–564. https://doi.org/10.1175/JPO2699.1

Redi, M. H. (1982). Oceanic isopycnal mixing by coordinate rotation. *Journal of Physical Oceanography*, *12*(10), 1154–1158. https://doi.org/10.1175/1520-0485(1982)012h1154:OIMBCRi2.0.CO;2

Roach, C. J., Balwada, D., & Speer, K. (2018). Global observations of horizontal mixing from Argo float and surface drifter trajectories. *Journal of Geophysical Research: Oceans*, *123*, 4560–4575. https://doi.org/10.1029/2018JC013750

Smith, K. S., & Marshall, J. (2009). Evidence for enhanced eddy mixing at middepth in the southern ocean. *Journal of Physical Oceanography*, *39*(1), 50–69. https://doi.org/10.1175/2008JPO3880.1

Stuut, J.-B. W., Prins, M. A., Schneider, R. R., Weltje, G. J., Jansen, J. F., & Postma, G. (2002). A 300-kyr record of aridity and wind strength in southwestern Africa: Inferences from grain-size distributions of sediments on Walvis Ridge, SE Atlantic. *Marine Geology*, *180*(1-4), 221–233. https://doi.org/10.1016/S0025-3227(01)00215-8

Talley, L. D. (2013). Closure of the global overturning circulation through the Indian, Pacific, and Southern Oceans: Schematics and transports. *Oceanography*, *26*(1), 80–97. https://doi.org/10.5670/oceanog.2013.07

Tulloch, R., Ferrari, R., Jahn, O., Klocker, A., LaCasce, J., Ledwell, J. R., et al. (2014). Direct estimate of lateral eddy diffusivity upstream of Drake Passage. *Journal of Physical Oceanography*, *44*(10), 2593–2616. https://doi.org/10.1175/JPO-D-13-0120.1

Vollmer, L., & Eden, C. (2013). A global map of meso-scale eddy diffusivities based on linear stability analysis. *Ocean Modelling*, *72*, 198–209. https://doi.org/10.1016/j.ocemod.2013.09.006